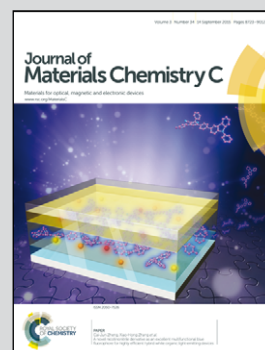


Showcasing research from Queensland Micro- and Nanotechnology Centre, Griffith University (Australia).

Graphite on paper as material for sensitive thermoresistive sensors

This work investigates the thermoresistive property of graphite on paper (GOP) fabricated by a pencil drawn on paper. The GOP shows a large temperature coefficient of resistance, which was utilised for a highly sensitive anemometer. The work demonstrates the feasibility of using the GOP for low-cost thermoresistive sensors.

As featured in:



See Toan Dinh *et al.*,
J. Mater. Chem. C, 2015, **3**, 8776.



www.rsc.org/MaterialsC

Registered charity number: 207890

CrossMark
click for updatesGraphite on paper as material for sensitive
thermoresistive sensors†Cite this: *J. Mater. Chem. C*, 2015,
3, 8776Received 5th June 2015,
Accepted 15th July 2015

DOI: 10.1039/c5tc01650a

www.rsc.org/MaterialsC

Toan Dinh,^{*a} Hoang-Phuong Phan,^a Dzung Viet Dao,^{ab} Peter Woodfield,^b
Afzaal Qamar^a and Nam-Trung Nguyen^a

This paper reports on the thermoresistive properties of graphite on paper (GOP). A negative temperature coefficient of resistance (TCR) from -2900 to -4400 ppm K^{-1} was observed for the GOP. This negative and large TCR is attributed to an increase in the thermionic emission current over a low potential barrier with increasing temperature. The potential barrier was found to be 33 meV between the graphite grains. The paper also demonstrates the use of the GOP in a highly sensitive (0.83 mV ($m s^{-1}$) $^{-0.8}$ mW^{-1}) GOP-based anemometer, indicating strong feasibility of using this material for low-cost and sensitive thermal sensing applications.

The thermoresistive effect has been widely utilized in thermal sensors with numerous successful applications such as flow sensors,^{1,2} inertial sensors,^{3,4} and temperature sensors.⁵⁻⁷ To date, various thermal sensing materials have been employed, including metals (platinum, nickel, copper, *etc.*) and semiconductors (silicon and polysilicon). Micromachining has successfully been used to fabricate thermal-based sensors, taking advantage of the maturity of microelectronics technology.³⁻⁹ However, the expensive materials, clean room facilities and specialised wafer processing equipment raise the cost of such devices, especially for small scale production.

Recent studies have paid a great deal of attention to paper-based devices for diagnostics, electronics and microfluidics applications.¹⁰⁻¹² The main advantages of this technology are the low cost, diversity in material choice, disposability and ease of fabrication.¹³ Graphite on paper (GOP), in which graphite layers are deposited on paper by either graphite-ink printing techniques,^{14,15} or manual pencil drawing techniques,¹⁶ has been utilized as the sensing element in flexible sensors for strain sensing and chemical analysis.¹⁶⁻¹⁹ Additionally, the excellent electrical conductivity of graphite and the low thermal conductivity

of porous paper make GOP an attractive material for thermoresistive sensors. Consequently, GOP, as a transducing element for thermal-based sensors, has remarkable advantages such as low cost, cleanroom-free fabrication and high sensitivity.

To the best of our knowledge, no work has been reported on the temperature dependence of electrical properties of GOP using pencil graphite on paper. Therefore, this work focuses on the thermoresistive property and conduction mechanism of the GOP material, and its application. We also demonstrate by using the example of an anemometer, the feasibility of using this material for thermoresistive sensors. The insights into the temperature dependence of GOP gained from this study could open a new perspective for the development of a range of paper-based thermal sensors.

The graphite on paper (GOP) material is created by hand drawing a 5B grade pencil line (Faber-Castell) on a paper sheet (Staples). The main components in the 5B grade pencil lead include 82 wt% graphite particles bound together by 12 wt% clay and 5 wt% wax.²⁰ The GOP material was cut into 20 mm \times 10 mm strips for the subsequent thermal characterization. 3M™ aluminum tape and low resistive silver epoxy (186-3616, RS Components) were employed as electrical readout pads. Fig. 1(a) shows a schematic sketch of the fabricated GOP mounted on a supporting base for thermoresistive property characterizations.

The properties of the GOP were then investigated utilizing optical measurements. Fig. 1(b) shows the scanning electron microscopy (SEM) image of the paper sheet, illustrating the cellulose fibres and the porosity of the paper. The SEM image of the pencil trace (Fig. 1(c)) also indicates that a continuous graphite film was deposited on the paper. In addition, Raman measurements were performed to characterize the defect quantity in the GOP. The Raman spectrum of the pencil trace (Fig. 1(d)) shows three main prominent peaks at the wavenumbers of 1350, 1580 and 2725 cm^{-1} corresponding to the D, G and 2D bands of graphite material, respectively.^{21,22} The level of the D-band peak is proportional to the number of defects and boundaries in the graphite trace, while the G band provides information about the sp^2 bonded carbon networks inside the graphite film.²¹

^a Queensland Micro-Nanotechnology Centre, Griffith University, Queensland, Australia. E-mail: toan.dinh@griffithuni.edu.au

^b School of Engineering, Griffith University, Queensland, Australia

† Electronic supplementary information (ESI) available: The impact of the thermal expansion and bending of the paper on the resistance change and the time response of the GOP-based anemometer. See DOI: 10.1039/c5tc01650a

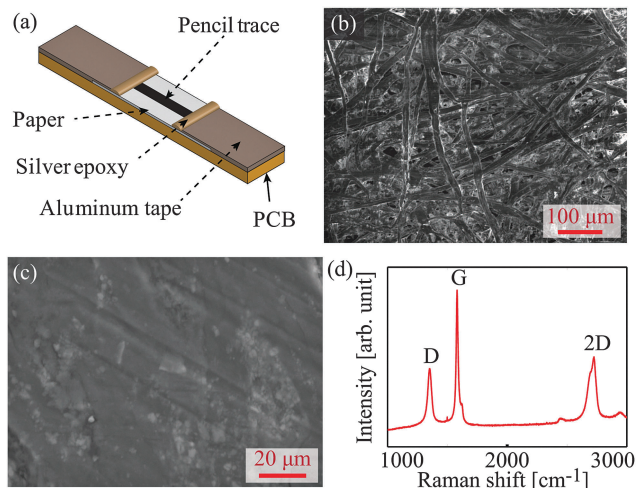


Fig. 1 Graphite on paper material: (a) schematic sketch of the graphite resistor (not to scale); (b) SEM image of the paper substrate; (c) SEM image of the pencil trace; (d) Raman spectrum of the pencil trace.

Additionally, the 2D band functions as an indication of stacking type in the direction perpendicular to the graphite plane. Based on the intensities of these bands, the average crystallite size L of the graphitic material can be estimated using the following equation:²³

$$L = 2.4 \times 10^{-10} \times \lambda^4 \times \left(\frac{I_D}{I_G}\right)^{-1} \quad (1)$$

where λ is the laser line wavelength used in the Raman measurements, and $\left(\frac{I_D}{I_G}\right) = 0.37$ is the ratio of the D and G band intensities. Consequently, the crystallite size L was calculated to be approximately 45 nm, which agrees with the range of 20 to 490 nm reported in ref. 23.

The linear current–voltage characteristic of the GOP was measured using a HP 4145B analyzer, indicating a good ohmic contact between the electrodes and the graphite trace (the inset Fig. 2(a)). The thermal characterization of the GOP was then performed in the temperature range of 300 to 380 K with an interval of 10 K in an oven (TD-330F model, Thermoline Scientific). The temperature inside the oven was monitored using a K-type thermocouple (resolution 1 °C, accuracy $\pm 3\%$), while the resistance of the GOP was measured by an ohmmeter (Fluke 117 true-rms multimeter, accuracy 0.1 Ω).

Fig. 2(a) shows the variation of the electrical resistance of the GOP with temperature. It can be seen that the resistance significantly decreased by approximately 24% when the temperature increased from 300 to 380 K. The change in the resistance of the GOP also showed good reproducibility in that, after raising the temperature to 380 K and then cooling it down to room temperature, the resistance of the GOP returned to its original value with an error of $\pm 0.5\%$. The decrease in the electrical resistance with increasing temperature indicates that the conduction of the GOP is thermally activated; this phenomenon can be explained as follows.

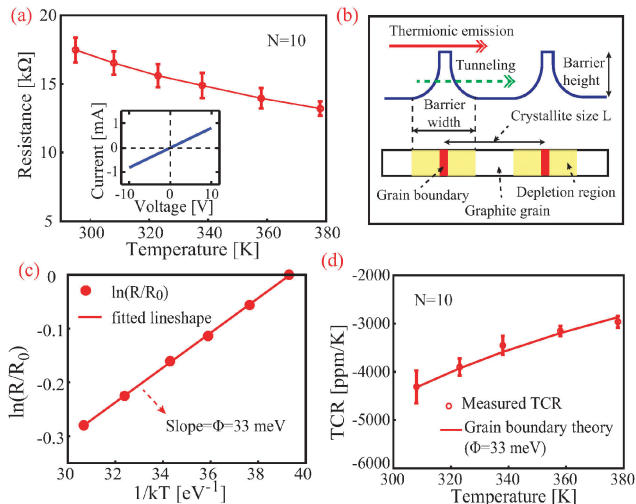


Fig. 2 Thermoresistive characteristics of the GOP: (a) electrical resistance versus temperature (number of samples $N = 10$; inset shows the I – V curve); (b) schematic sketch of graphite grains and potential barriers at their boundaries; (c) Arrhenius plot of GOP thermoresistance; (d) temperature coefficient of resistance (TCR).

When the temperature changes, the thermal expansion and bending of the paper and the change of GOP resistivity contribute to the resistance change of the GOP.²⁴ The maximum relative resistance change $\Delta R/R$ of the GOP due to the thermal expansion and bending of the paper was respectively estimated to be approximately 1.2% and 1.8% at 380 K (ESI[†]). These contributions are much smaller than the total resistance change (24%). Therefore, the thermal expansion and bending of the paper have a small influence on the resistance change and can be neglected.

Consequently, the decrease in the electrical resistance is mainly caused by the temperature dependence of GOP resistivity. It is believed that the resistance of the graphite trace comes from graphite grain resistance and their boundary resistance.^{25,26} Due to the large number of defects $\left(\frac{I_D}{I_G}\right) = 0.37$, free carriers are trapped in the boundaries between graphite grains, creating a potential barrier Φ which impedes the motion of carriers from one graphite grain to another grain (Fig. 2(b)). Since the resistance of graphite grains is much smaller than that of boundaries,^{27,28} the GOP resistance can be approximated as the boundary resistance, which is expressed in the following form:

$$R \sim \exp\left(\frac{\Phi}{kT}\right) \quad (2)$$

where k is the Boltzmann constant. Therefore, the relationship between the resistance change and the temperature can be expressed as:

$$\ln(R/R_0) = \frac{\Phi}{kT} - b \quad (3)$$

where $b = \Phi(kT_0)^{-1}$ is a constant (R_0 is the GOP resistance at the reference temperature T_0). From the slope of $\ln(R/R_0)$ versus $1/kT$ shown in Fig. 2(c), the barrier height, Φ , was found to be approximately 33 meV. This result is comparable to that (5 to 34 meV)

attributed to a polysilicon material²⁹ which also has boundary structures. We hypothesize that when the temperature increases, the thermally excited carriers can pass through the barrier by quantum-mechanical tunneling. They can also move over the barrier by thermionic emission. However, due to the low potential barrier ($\Phi = 33$ meV), the thermionic emission is considered as the dominant contribution to the significant decrease in the electrical resistance of the GOP.^{29,30} The resistance change of the GOP is then quantified using the temperature coefficient of resistance (TCR) which is defined in the following equation:

$$\text{TCR} = \frac{1}{R} \frac{dR}{dT} = -\frac{\Phi}{kT^2} \quad (4)$$

The measured TCR ranges from -2900 ppm K^{-1} to -4400 ppm K^{-1} , which is comparable to that of common temperature sensing materials such as platinum (3920 ppm K^{-1}), copper (4300 ppm K^{-1}) and nickel (6810 ppm K^{-1}).⁸ Based on eqn (4) and the defined Φ value, the well fitted TCR function is shown in Fig. 2(d). The large TCR obtained in this study indicates that the GOP is a good candidate for thermal-based applications such as GOP anemometers which will be presented hereafter.

A GOP-based anemometer was fabricated utilizing the same method as mentioned in the previous section. A cavity beneath the GOP was formed to thermally insulate the paper from the substrate. Fig. 3(a) shows an image of the fabricated anemometer. The working principle of the fabricated GOP anemometer is the same as that of conventional thermal flow sensors.³¹ That is, when constant heating power is applied to the GOP, the temperature of the GOP heater increases as a result of the Joule heating effect. As the air flow surrounding the heater increases, the convective heat loss from the heater increases, leading to the decrease of its temperature. As a result, the resistance of the GOP increases owing to its negative TCR. By detecting the resistance change of the sensor, the air flow velocity can be determined. In this study, the resistance change of the GOP was detected by applying a constant current and measuring the differential output voltage.

In order to monitor the output voltage of the sensor, the four-point measurement was employed as shown in Fig. 3(b).

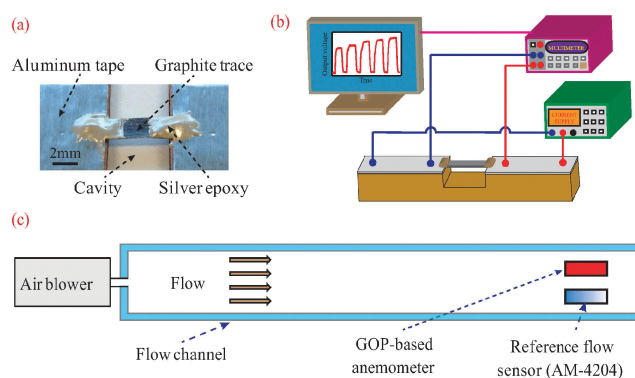


Fig. 3 Flow measurement: (a) fabricated GOP anemometer; (b) schematic sketch of four-point measurement setup (not to scale); (c) schematic sketch of flow measurement setup (not to scale).

A USB modular source measurement unit (Agilent U2722A) was utilized as the current supply and the multimeter. Fig. 3(c) shows the schematic diagram of the experimental setup for flow measurement. An air blower (LB0115-002, Industrial Equipment and Control) generated air flow ranging from 1 to 4 m s^{-1} at room temperature (23 °C), while a hot wire anemometer (AM-4204, RS Components) was used as a reference flow sensor.

The Reynolds number $Re = D\nu\rho/\mu$ of the setup varied from approximately 6500 to 26000 when the flow velocity ν changed from 1 m s^{-1} to 4 m s^{-1} . The diameter of the flow channel pipe D is 10 cm, ρ and μ are the density and viscosity of air, respectively. The high Reynolds number indicates that the flow passing the GOP sensor was turbulent.³² We evaluated the impact of the strain induced by the air flow, by measuring the resistance of unheated GOP anemometer at different flow velocities. The resistance of the GOP anemometer showed a very small change of less than 0.1% when applying a maximum air flow velocity of 4 m s^{-1} . This result indicates that the influence of the strain induced by the air flow on the output signal of the anemometer can be neglected.

The voltage across the GOP sensor was measured for different air velocities and at a constant current of 10 mA, shown in Fig. 4. It is evident that the output voltage increased significantly with increasing air flow rate, which is due to the fact that the hot-film GOP anemometer operates based on the heat transfer from the graphite-trace heater to surrounding air as mentioned in the previous section. Furthermore, the resistance of the GOP increased with increasing air flow rate and returned to the initial value when the air flow rate equaled zero, indicating a very good reversible characteristic of the GOP. The response of the sensor to different flow velocities was also measured at different constant currents of 8 and 6 mA, Fig. 5. In the constant-current mode, the differential output voltage ΔV and flow velocity ν follow King's law:

$$\Delta V = a + b\nu^n \quad (5)$$

where a , b and n are empirical constants.⁸ Fig. 5 indicates the highest sensitivity (0.83 mV $(\text{m s}^{-1})^{-0.8}$ mW^{-1}) of the GOP sensor at a constant current of 10 mA and a power consumption of 120 mW. This sensitivity is almost 1.2 times higher than that of a hot-film sensor made of platinum as reported previously

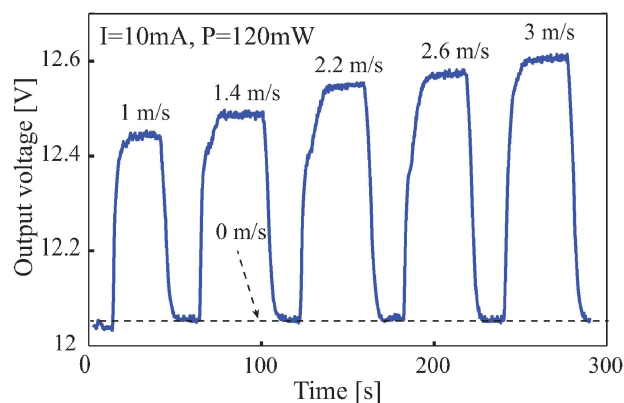


Fig. 4 The response of the GOP anemometer to different air flow velocities.

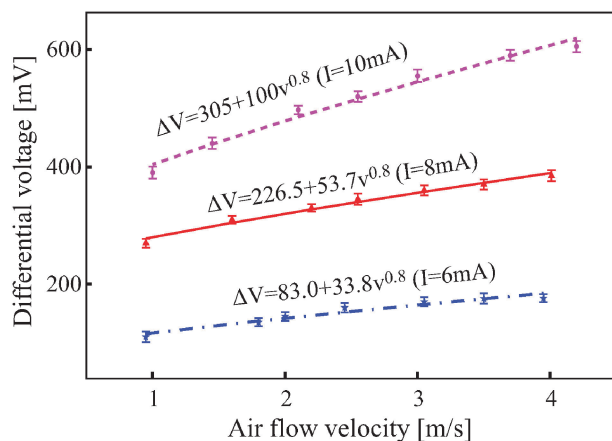


Fig. 5 Performance of the GOP anemometer at different applied constant currents.

in ref. 9. The high TCR of the GOP and the low thermal conductivity of the porous paper³³ (approximately $0.1 \text{ W m}^{-1} \text{ K}^{-1}$) clearly improve the performance of the GOP anemometer. The time response of the anemometer was also investigated at room temperature ($23 \text{ }^\circ\text{C}$) in quiescent air and under atmospheric pressure.³⁴ The obtained result indicates that the 90% response time of the GOP anemometer is approximately 2.3 s (ESI[†]), which is comparable to that of other thermal flow sensors.³¹

In conclusion, the thermoresistive property and conduction mechanism of the GOP were investigated. The application of the GOP for flow measurement was also demonstrated. The high TCR of the GOP from -2900 ppm K^{-1} to -4400 ppm K^{-1} was found for the temperature range of 300 to 380 K. The GOP anemometer displayed a relatively high sensitivity of $0.83 \text{ mV (m s}^{-1}\text{)}^{-0.8} \text{ mW}^{-1}$, demonstrating a good feasibility of using GOP for highly sensitive and low-cost paper-based thermoresistive sensors.

This work was performed in part at the Queensland node of the Australian National Fabrication Facility, a company established under the National Collaborative Research Infrastructure Strategy to provide nano and micro-fabrication facilities for Australia's researchers. This work has been partially supported by the Griffith University's New Researcher Grants.

References

- D. Hamadi, B. Garnier, H. Willaime, F. Monti and H. Peerhossaini, *Lab Chip*, 2012, **12**(3), 652–658.
- N. T. Nguyen, *IEEE Sens. J.*, 2005, **5**, 1224–1234.
- V. T. Dau, D. V. Dao and S. Sugiyama, *Smart Mater. Struct.*, 2007, **16**, 2308–2314.
- D. V. Dao, V. T. Dau, T. Shiozawa and S. Sugiyama, *J. Microelectromech. Syst.*, 2007, **16**, 950–958.
- C. Yan, J. Wang and P. S. Lee, *ACS Nano*, 2015, **9**(2), 2130–2137.
- C. Yu, Z. Wang, H. Yu and H. Jiang, *Appl. Phys. Lett.*, 2009, **95**(14), 141912.
- T. Dinh, D. V. Dao, H. P. Phan, L. Wang, A. Qamar, N. T. Nguyen, P. Tanner and M. Rybachuk, *Appl. Phys. Express*, 2015, **8**, 061303.
- J. T. W. Kuo, L. Yu and E. Meng, *Micromachines*, 2012, **3**, 550–573.
- F. Mailly, A. Giani, R. Bonnot, P. Temple-Boyer, F. Fascal-Delannoy, A. Foucaran and A. Boyer, *Sens. Actuators, A*, 2001, **94**, 32–38.
- X. Cai, M. Peng, X. Yu, Y. Fu and D. Zou, *J. Mater. Chem. C*, 2014, **2**(7), 1184–1200.
- Z. Nie, F. Deiss, X. Lui, O. Akbulut and G. M. Whitesides, *Lab Chip*, 2010, **10**, 3163–3169.
- P. J. Bracher, M. Gupta and G. M. Whitesides, *J. Mater. Chem.*, 2010, **20**, 5117–5122.
- S. K. Mahadeva, K. Walus and B. Stoeber, *ACS Appl. Mater. Interfaces*, 2015, **7**, 8345–8362.
- T. Akter, J. Joseph and W. S. Kim, *IEEE Electron Device Lett.*, 2012, **33**(6), 902–904.
- X. Liu, M. Mwangi, X. Li, M. O'Nrien and G. M. Whitesides, *Lab Chip*, 2011, **11**(13), 2189–2196.
- C. W. Lin, Z. Zhao, J. Kim and J. Huang, *Sci. Rep.*, 2014, **4**, 3812.
- X. Liao, Q. Liao, X. Yan, Q. Liang, H. Si, M. Li and Y. Zhang, *Adv. Funct. Mater.*, 2015, **25**(16), 2395–2401.
- H. P. Phan, D. V. Dao, T. Dinh, H. Brooke, A. Qamar, N. T. Nguyen, Y. Zhu, *Proc. 28th IEEE Int. Conf. Micro Electro Mechanical Systems (MEMS)*, Estoril, 2015, pp. 825–828.
- T. K. Kang, *Appl. Phys. Lett.*, 2014, **104**, 073117.
- M. C. Sousa and J. W. Buchanan, *Comput. Graph. Forum*, 2000, **19**, 27–49.
- M. A. Pimenta, G. Dresselhaus, M. S. Dresselhaus, L. G. Cancado, A. Jorio and R. Saito, *Phys. Chem. Chem. Phys.*, 2007, **9**, 1276–1290.
- F. Tuinstra and J. L. Koenig, *J. Phys. Chem.*, 1970, **53**, 1126.
- L. G. Cancado, K. Takai, T. Enoki, M. Endo, Y. A. Kim, H. Mizusaki and M. A. Pimenta, *Appl. Phys. Lett.*, 2006, **88**(16), 163106.
- J. Borch, M. B. Lyne, R. E. Mark and C. Habeger, *Thermal properties, Handbook of physical testing of paper*, Taylor and Francis, 2001, ch. 10, pp. 400–404, ISBN: 978-082-4707-86-6.
- T. R. Albrecht, H. A. Mizes, J. Nogami, S. I. Park and C. F. Quate, *Appl. Phys. Lett.*, 1988, **52**(5), 362–364.
- Y. Gan, W. Chu and L. Qiao, *Surf. Sci.*, 2003, **539**(1), 120–128.
- J. Li, R. Jia, X. Tang, X. Zhao and S. Li, *J. Phys. D: Appl. Phys.*, 2013, **46**, 325304.
- H. Y. Lee, L. C. Burton, *Proc. 8th IEEE Int. Sym. Applications of Ferroelectrics*, Greenville, 1992, pp. 98–102.
- J. Y. Seto, *J. Appl. Phys.*, 1975, **46**, 5247–5254.
- M. S. Raman, T. Kifle, E. Bhattacharya and K. N. Bhat, *IEEE Trans. Electron Devices*, 2006, **53**(8), 1885–1892.
- N. T. Nguyen, *Flow Meas. Instrum.*, 1997, **8**(1), 7–16.
- J. M. Ma, S. H. Peng, L. Davidson and F. J. Wang, *Int. J. Heat Fluid Flow*, 2011, **32**(3), 652–669.
- Z. T. Yu, X. Xu, L. W. Fan, Y. C. Hu and K. F. Cen, *For. Prod. J.*, 2010, **61**, 130–135.
- T. Neda, K. Nakamura and T. Takumi, *Sens. Actuators, A*, 1996, **54**(1), 626–631.